Investigation of the co-crystallisation of N-heterocycles

By

Leigh-Anne Loots

Thesis presented in partial fulfilment of the requirements for the degree of Master of Science

at

Stellenbosch University

Department of Chemistry and Polymer Science

Faculty of Science

Supervisor: Leonard J. Barbour

March 2009

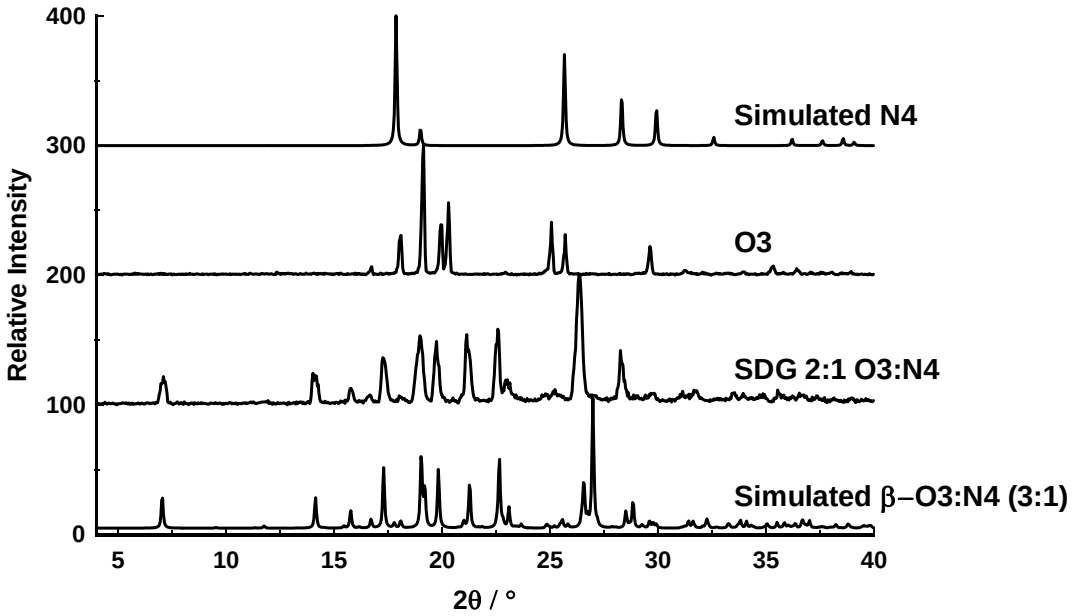

Figure 3.86 PXRD pattern from a 2:1 O3:O4 SDG experiment, compared to the simulated pattern of *β*–O3N4 and the two pure components.

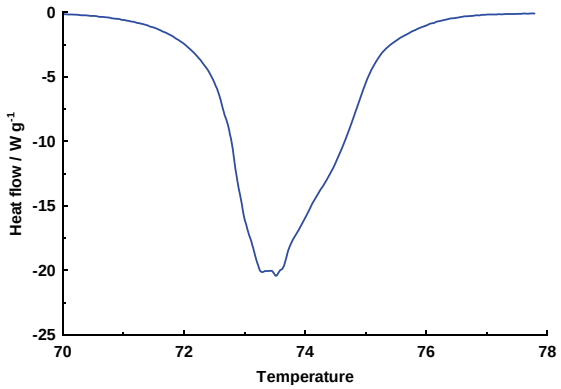

Figure 3.87 DSC trace of *β*–O3N4

3.2.9 O4N4 – Hydroquinone pyrazine (1:1 ratio)

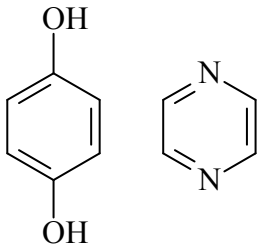

Scheme 3.15 Co-crystal formers hydroquinone and pyrazine

O4N4 crystallises in the monoclinic space group $P2_1/c$. The ASU (Figure 3.88) consists of half molecules each of hydroquinone and pyrazine, located on inversion centres at the origin and $\frac{1}{2},\frac{1}{2},0$ respectively. Molecules are connected *via* the OH⋯N_{arom} synthon to form 1-D polymeric chains, $C_2^2(12)$. The structure of O4N4 is relatively simple, comprising 1-D chains that form layers along the *a* axis that are held in place by weak C–H⋯O interactions. The fingerprint plot (Figure 3.89) depicts these interactions by the shorter inner tails, while outer tails represent the OH⋯N hydrogen bonds. Adjacent layers stack in an ABAB pattern such that, when viewed along [001], the pattern is reminiscent of that produced in γ-hydroquinone as well as α–O4N2 structures (Figure 3.90). Although the actual H–bond connectivity of O4N4 is different to that in the other structures, the arrangement of the hydroquinone molecules is essentially the same.

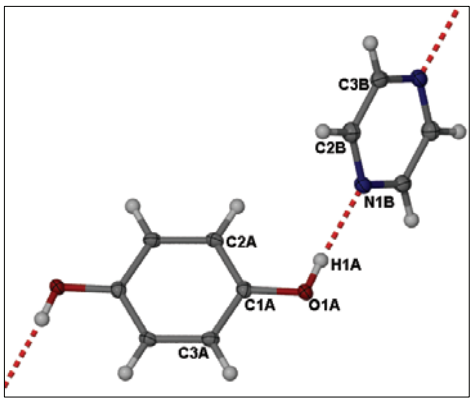

Figure 3.88 Thermal ellipsoid plot of the ASU of O4N4. Only ASU atoms are labelled

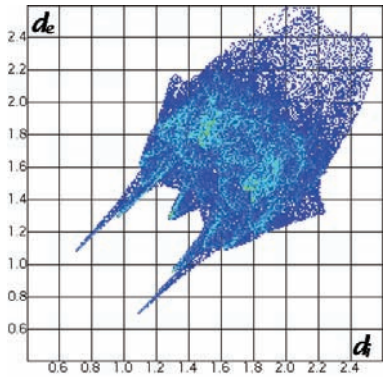

Figure 3.89 Fingerprint plot of O4N4.

At first glance it is difficult to establish the differences between the packing arrays of the structures of α–O4N2 and O4N4 (Figure 3.90). The remarkable similarity results from the orientation of the hydroquinone molecules in the 3-D array, maintaining the same position down vertical columns in both structures (red molecules). Horizontally, hydroquinone molecules are orientated differently – in the α–O4N2 structure molecules alternate, while in O4N4 they are aligned in the same direction. In both structures, hydroquinone has allowed diazine molecules to intersperse between them, thus allowing the heterosynthon OH⋯N_{arom} to form in place of OH⋯O homosynthons. The slight differences between the two structures shown in Figure 3.90 are produced by the different positions on the N-atom about the

heterocycles (*ortho* and *para* diazine rings). It can thus be said that the acceptor molecules have a directing effect on the relatively robust structure of *γ*-hydroquinone.

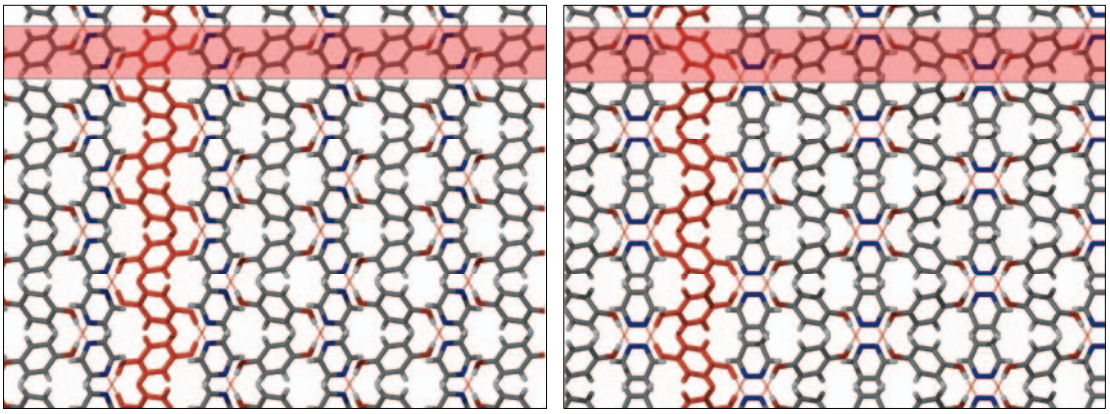

Figure 3.90 Structures of O4N4 on the left and *α*–O4N2 on right. The red shaded area shows the alignment of the hydroquinone molecules brought about by hydrogen bonding with the respective diazine molecules. Red molecules show the similar orientation of hydroquinone molecules.

The PXRD pattern for O4N4 can be reproduced by a SDG experiment using 1:1, 1:2 or 2:1 molar ratios of O4:N4 (Figure 3.91). The 2:1 molar ratio shows residual peaks of the excess hydroquinone. The DSC analysis produces a single thermal event (T_{on} = 128 °C), which is the highest melting point of all the co-crystals investigated in this study, and the only one that undergoes a phase change above 100 °C (Figure 3.92).

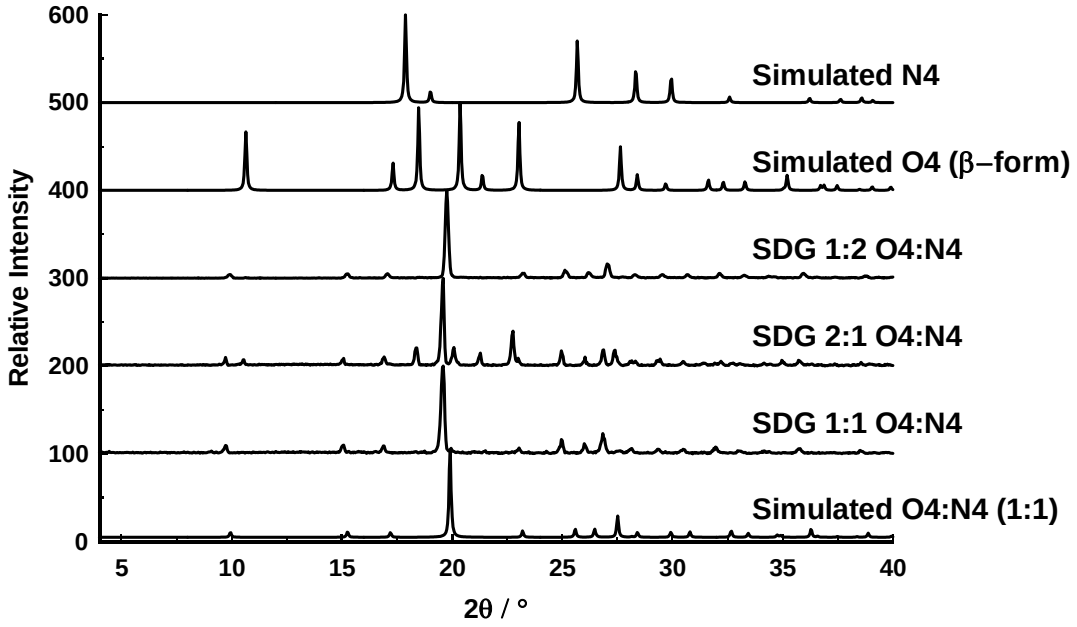

Figure 3.91 PXRD patterns for the 1:1, 1:2 and 2:1 molar ratio SDG experiments compared to the simulated O4N4 pattern and the two pure components.

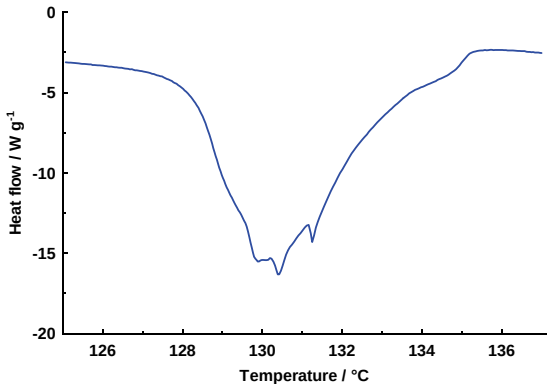

Figure 3.92 DSC trace of O4N4

To conclude the analysis of the co-crystals of this 3×3 grid, a PXRD comparison of three co-crystal structures is included (Figure 3.93). During the course of this chapter, similarities between structures showing similar packing arrangements have been addressed, although hydrogen-bonding patterns have differed. The simulated PXRD data provides us with a more experimental representation of the similarities between the atomic coordinates of the structures. It is evident from these data that *α*–O4N2 and O4N4 are most alike. However, O3N2 differs only slightly from these two. The fingerprint plots (Figure 3.94) of the three co-crystals are also compared, and provides further evidence that *α*–O4N2 is more similar to O4N4 than it is to O3N2.

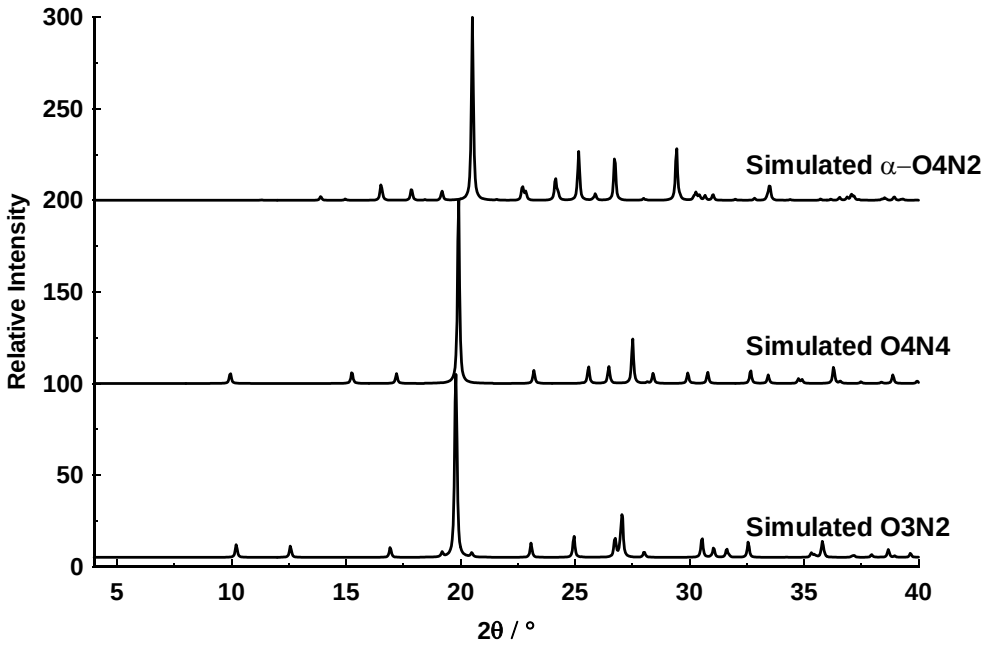

Figure 3.93 Comparison of the simulated PXRD patterns for α–O4N2, O4N4 and O3N2.

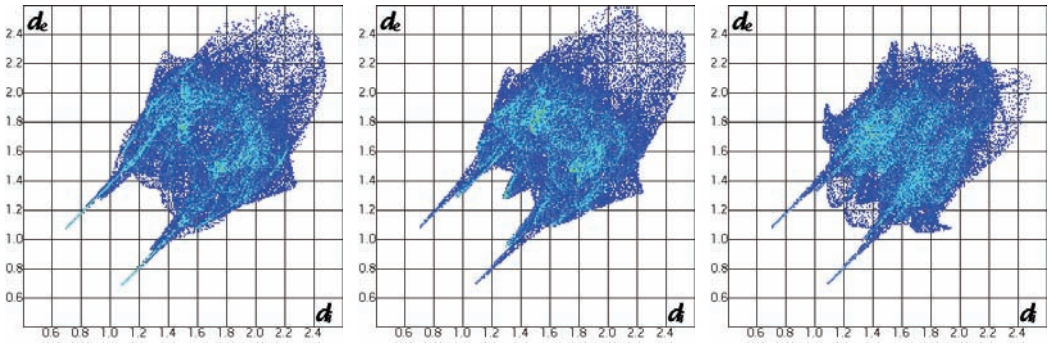

Figure 3.94 Comparison of the fingerprint plots of co-crystals α –O4N2 (left), O4N4 (middle) and O3N2 (right).

Summary and discussion

Structural flexibility observed in the three benzenediol isomers is an important aspect in the formation of the co-crystal structures reported here. Flexibility of the hydroxyl functional groups of these molecules leads to the possibility of different hydrogen bonding networks, depending on the nature of the hydrogen bonded acceptor molecule. Although the co-crystals in this study represent only a small fraction of co-crystals, and a statistical study would be dramatically skewed, there are noticeable preferences for the conformation of both catechol and hydroquinone in the these compounds. Catechol (O2) favours the *syn–anti* over the *anti–anti* conformation, while hydroquinone (O4) is predominantly in the *trans*-conformation. Conformation of resorcinol (O3) is equally distributed between the three possibilities – *anti–anti*, *syn–anti* and *syn–syn*. A CSD survey revealed that approximately 60% of the catechol-containing organic structures (22 structures) in the CSD exhibit the *syn–anti* conformation.[23] Of the 112 structures retrieved from the CSD containing hydroquinone, approximately 90% contain the *trans*–conformation.[23] Resorcinol co-crystals retrieved from the CSD follow a similar trend to that observed in this study, with an approximately equal distribution of the three conformations.[23] The structures of all diazine molecules display offset π⋯π stacking interactions between aromatic rings supported by C–H⋯N interactions.

Of the thirteen structures reported here, the 1:1 molar ratio is most significant (seven structures). These 1:1 molar ratio structures form either discrete quaternary adducts (O2N3, *α*–O3N4, O4N3) or infinite chains (*α*–O4N2, O4N3 and O4N4). Structures containing an excess of the diazine molecule (*β*–O2N2 and *β*–O4N2), have only one N-atom acceptor involved in strong hydrogen bonds, while the other participates in weaker C–H⋯N interactions. The close proximity of the N–atoms about the diazine ring is arguably the cause of this unsaturated conformation. Interestingly, these two structures both contain the same diazine molecule, pyridazine, and are remarkably similar in their 2-D packing arrangements.

Four co-crystal structures have been obtained from catechol and the three diazine isomers. Two different forms were prepared from pyridazine (*α*–O2N2 and *β*–O2N2). The *α*–form is a 2:1 hexa–adduct that resembles a distorted paddlewheel, while *β*–O2N2 consists of 1:2 ternary adducts. The structure of O2N3 forms from quaternary adducts that pack in a herringbone motif. The 2:1 chains of O2N4 also form a herringbone motif.

Five co-crystal structures containing resorcinol (O3) were obtained in this 3×3 grid. The two structures obtained from pyrimidine closely resembled one another both forming 1:1 chains with resorcinol in the *syn–anti* conformation. The *β*–form contains an additional resorcinol molecule, which adopts the *syn–syn* conformation to act as a pincer, maintaining the positions of two adjacent chains. The two structures prepared with pyrazine yield two very different 3-D architectures. Quaternary hydrogen-bonded adducts are formed in the designated *α*–form, with resorcinol in the *syn–syn* conformation. The *β*–form, however, features three independent 3-D interpenetrated ladders. The final resorcinol co-crystal O3N2 shares a slight similarity with the structure of pure resorcinol, as well as with that of *α*–O4N2.

Hydroquinone provides the most interesting series of co-crystals. Similarly to catechol, two contrasting hydrogen bonding motifs were obtained when co-crystallised with pyridazine. In this instance, the *α*–form consists of 1:1 hydrogen bonded chains that are show remarkably similar to those formed in O3N2. The *β*–form, on the other hand, forms 1:2 ternary adducts with pyridazine. These adducts pack in a manner similar to those in *β*–O2N2.

Undoubtedly, the most intriguing result of this 3×3 grid is the structure of O4N3. Owing to the position of the molecules on sites of symmetry, the hydrogen-bonding pattern cannot be established by crystallography alone. Two possible motifs exist: either discrete hydrogen bonded quaternary rings or 1:1 hydrogen bonded chains. Theoretical modelling of the two scenarios does not provide substantiating evidence regarding an energy preference for the one motif over the other. It is anticipated that results, still pending, from MAS-NMR will provide data that favour one motif over the other. The final structure in this 3×3 grid is that of O4N4, which forms 1:1 hydrogen bonded chains. Although the hydrogen-bonding motif is slightly different to that observed in the structure of α–O4N2, the arrangement of the molecules in 3-D is similar in these two structures.

Table 3.2 Crystallographic Data of Co-Crystals O2N2 – O3N3 (α)

	α–O2N2	**β–O2N2**	**O3N2**	**α–O4N2**	**β–O4N2**	**O2N3**	**α–O3N3**
Molecular, Empirical formula	$C_{16}H_{16}N_2O_4$ $2(C_6H_6O_2)\cdot(C_4H_4N_2)$	$C_{14}H_{12}N_4O_2$ $(C_6H_6O_2)\cdot 2(C_4H_4N_2)$	$C_{10}H_{10}N_2O_2$ $(C_6H_6O_6)\cdot(C_4H_4N_2)$	$C_5H_5N_1O_1$ $½(C_6H_6O_2)\cdot ½(C_4H_4N_2)$	$C_7H_7N_2O_1$ $½(C_6H_6O_2)\cdot(C_4H_4N_2)$	$C_{10}H_{10}N_2O_2$ $(C_6H_6O_2)\cdot(C_4H_4N_2)$	$C_{10}H_{10}N_2O_2$ $(C_6H_6O_2)\cdot(C_4H_4N_2)$
OH:N ratio	2:1	1:2	1:1	1:1	1:2	1:1	1:1
M_r/ g.mol^{-1}	300.31	268.28	190.20	190.20	135.15	190.20	190.20
Crystal Symmetry	Monoclinic	Monoclinic	Orthorhombic	Monoclinic	Monoclinic	Monoclinic	Triclinic
Space Group	$P2_1/c$	$P2_1/c$	$P2_12_12_1$	$C2/c$	$P2_1/c$	$P2_1/n$	$P\bar{1}$
a/Å	8.494(1)	11.379(2)	7.366(2)	18.706(5)	6.162(1)	5.829(1)	6.966(3)
b/Å	14.217(1)	16.393(3)	9.925(3)	7.701(2)	16.363(2)	21.962(4)	6.978(3)
c/Å	12.430(1)	7.149(1)	12.681(4)	7.131(2)	7.102(1)	7.545(1)	10.555(5)
α/°	90	90	90	90	90	90	90.208(7)
β/°	99.121(2)	96.558(7)	90	112.183(4)	114.186(3)	112.279(3)	91.138(7)
γ/°	90	90	90	90	90	90	118.781(7)
Z	4	4	4	4	4	4	2
V/Å^3	1482.05	1324.76	927.08	951.20	653.30	893.62	449.59
T /K	173	100	100	100	100	100	100
D_{calc} /g cm^{-3}	1.3457	1.3550	1.3625	1.3280	1.3738	1.4135	1.4048
N-total	9325	3270	5638	2976	4196	10405	5013
N-independent	3235	3150	1224	1096	1529	2132	2047
N-observed	1931	2207	1106	847	1318	1812	1632
R_1 [I>2σ(I)]	0.0466	0.0759	0.0466	0.0588	0.0417	0.0575	0.1167
wR_2	0.1015	0.1605	0.0929	0.1250	0.1087	0.1206	0.3022
GOF	0.916	1.077	0.1022	1.126	1.042	1.117	1.245

Table 3.2 (cont.) Crystallographic data of co-crystals O3N3 (β) – O4N4

	β–O3N3	**O4N3**	**O2N4**	**α–O3N4**	**β–O3N4**	**O4N4**
Molecular, Empirical formula	$C_{16}H_{16}N_2O_4$ $2(C_6H_6O_2)\cdot(C_4H_4N_2)$	$C_5H_5N_2O_1$ $½(C_6H_6O_2)\cdot½(C_4H_4N_2)$	$C_{16}H_{16}N_2O_4$ $2(C_6H_6O_2)\cdot(C_4H_4N_2)$	$C_{10}H_{10}N_2O_2$ $(C_6H_6O_2)\cdot(C_4H_4N_2)$	$C_{22}H_{22}N_2O_6$ $3(C_6H_6O_2)\cdot(C_4H_4N_2)$	$C_5H_5N_1O_1$ $½(C_6H_6O_2)\cdot(C_4H_4N_2)$
OH:N ratio	2:1	1:1	2:1	1:1	3:1	1:1
M_r/ g.mol^{-1}	300.31	190.20	300.31	190.20	410.43	95.10
Crystal Symmetry	Monoclinic	Monoclinic	Orthorhombic	Monoclinic	Monoclinic	Monoclinic
Space Group	$P2_1/c$	$C2/c$	$Pbca$	$P2_1/n$	$P2_1/n$	$P2_1/c$
a/Å	10.642(3)	18.381(2)	10.588(1)	7.523(2)	8.066(1)	8.887(1)
b/Å	10.473(3)	7.752(1)	14.796(1)	15.841(4)	25.010(4)	7.660(1)
c/Å	13.290(4)	6.673(1)	18.591(2)	8.191(2)	10.201(2)	6.957(1)
α/°	90	90	90	90	90	90
β/°	97.385(4)	93.716(2)	90	107.384(4)	102.586(3)	90.014(2)
γ/°	90	90	90	90	90	90
Z	4	4	8	4	4	4
V/Å^3	1468.97	948.83	2912.64	932.14	2008.44	473.60
T /K	100	100	100	100	100	100
D_{calc} /g cm^{-3}	1.3577	1.5414	1.3695	1.3551	1.3571	1.3336
N-total	9105	5407	34004	10921	12423	3042
N-independent	3408	1119	3568	2241	4634	1104
N-observed	2319	834	3152	1865	3054	1013
R_1 [I>2σ(I)]	0.1043	0.0465	0.0827	0.0582	0.819	0.0391
wR_2	0.2084	0.1321	0.1772	0.1188	0.1458	0.1048
GOF	1.132	1.359	1.187	1.103	1.057	1.056

REFERENCES

1. F. Allen, *Acta Crystallogr., Sect. B*, 2002, **58**, 380-388.
2. F. R. Fronczek, K. K. Kim and R. M. Strongin, 2002, *CSD* as a private communication to the CSD, Refcode *CATCOL13*.
3. T. J. Mooibroek, P. Gamez and J. Reedijk, *CrystEngComm*, 2008, **10**, 1501-1515.
4. F. R. Fronczek, 2001, CSD in a private communication to the CSD, Refcode *RESORA03*,
5. J. M. Robertson and A. R. Ubbelohde, *Proc. Royal Soc. London. Series A, Mathematical and Physical Sciences*, 1938, **167**, 136-147.
6. T. Friščić and L. R. MacGillivray, *Mol. Cryst. Liq. Cryst.*, 2006, **456**, 155-162.
7. V. R. Thalladi, H. C. Weiss, R. Boese, A. Nangia and G. R. Desiraju, *Acta Crystallogr., Sect. B*, 1999, **55**, 1005-1013.
8. T. C. W. Mak and C.-K. Lam, Hydroquinone, in *Encyclopedia of Supramolecular Chemistry*, eds. J. L. Atwood and J. W. Steed, Marcel Dekker, Inc., New York; Basel, 2004, vol. 1, pp. 679-686.
9. M. Bolte and H.-W. Lerner, 2001, CSD in a private communication to the CSD, Refcode *HYQUIN06*.
10. S. C. Wallwork and H. M. Powell, *J.C.S. Perkin II* 1980, 641-646.
11. S. V. Lindeman, V. E. Shklover and Y. T. Struchkov, *Cryst. Struct. Commun.*, 1981, **10**, 1173.
12. K. Maartmann-Moe, *Acta Crystallogr.*, 1966, **21**, 979.
13. A. J. Blake and D. W. H. Rankin, *Acta Crystallogr., Sect. C*, 1991, **47**, 1933.
14. S. Furberg, J. Grogaard and B. Smedsrud, *Acta Chem. Scand. B*, 1979, **33**, 715.
15. G. de With, S. Harkem and D. Feil, *Acta Crystallogr., Sect. B*, 1976, **32**, 3178.
16. M. C. Etter, *Acc. Chem. Res.*, 1990, **23**, 120-126.
17. L. R. MacGillivray, *J. Org. Chem.*, 2008, **73**, 3311-3317.

CHAPTER 4

Co-crystals of Benzenediol and Benzodiazine Isomers

Introduction

In order to further the investigation into the O–H⋯N supramolecular synthon and other subtle interactions involved in the self-assembly of organic molecules in the solid-state, a second 3×3 grid of co-crystal compounds is presented here. This grid is closely related to that reported in Chapter 3. The monocyclic hydrogen bond acceptor molecules, in this instance, have been replaced by bicyclic benzodiazine isomers. These isomers have identical nitrogen positioning about one aromatic ring, with *ortho*, *meta* and *para* isomers possible. A benzene ring is fused to these diazine rings at the 5 and 6 positions, resulting in extended aromaticity over the bicyclic ring. Modification to the ring size is not expected to affect the formation of strong hydrogen bonds *via* the OH⋯N heterosynthon. This is because the bicyclic diazine molecules have been shown[1] to exhibit similar reactivities to the monocyclic diazines. Both the monocyclic and bicyclic heteroaromatic molecules follow a near identical trend of decreasing basicity as the N–atoms become more remote from each other about the ring. Owing to an increased aromatic area, the weaker π⋯π interactions are expected to be more favourable for the larger bicyclic molecules compared to edge-to-face interactions preferred in the smaller monocyclic varieties.

Crystal engineering utilizing hydrogen bonding relies on an understanding of both strong and weak intermolecular interactions. Therefore the effect of the increased aromaticity of the bicyclic acceptor molecules can be compared to the structures obtained in the first 3×3 grid. The co-crystal structures obtained for the second grid, reported here, enables comparisons to be made with related structures of the grid presented in Chapter 3. If there is a prevalence of offset π⋯π interactions in the second grid, much needed information will be provided with regard to the subtle balance between strong and weak intermolecular interactions in the solid-state.

The benzodiazine molecules are currently employed as a backbone for the preparation of a number of pharmaceutical compounds. Modified quinazoline has been used in anti-malarial and cancer treatments and quinoxaline in antibiotics such as echinomycin. Their propensity to form co-crystals is significant for improvements to the current and future formulations of these pharmaceutical preparations. As mentioned in Chapter 1, co-crystals provide the opportunity for improved solubility, stability etc. of APIs employed in prescription drugs. Therefore, this investigation of co-crystals of benzodiazine isomers could have a direct impact on the preparation of some of these pharmaceuticals currently on the market.

The hydrogen bond donors used in the preparation of the co-crystals reported here are the same as those of the previous grid and the reader is referred to Chapter 3 for more information on these compounds. The structures of the benzodiazine isomers were retrieved from the CSD, except for the structure of phthalazine, which was collected by the author. All three structures are discussed briefly prior to discussion of the eight co-crystal structures obtained in this study.

Crystallographic data for each of the co-crystals described here are provided in (Table 4.2). The Crystallographic Information Files, included for each structure, provide information regarding the atomic coordinates, bond lengths and angles, torsion angles, thermal parameters and hydrogen bonding parameters, and can also be found in the Appendices. Intermolecular bond distances and θ angles for each structure are also available in the Appendices.

4.1 Starting Materials

4.1.1 BN23 – Phthalazine (2,3 – benzodiazine)

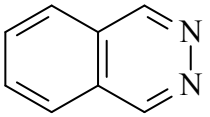

Scheme 4.1 Phthalazine

The single-crystal structure of phthalazine has not been reported to date, which is somewhat surprising because the compound is readily available in its solid form. However, single crystals of suitable quality for SCD analysis are difficult to grow. Although the structure reported here is not of high quality, it does provide information regarding the interactions involved in the 3-D arrangement of the molecules.

Phthalazine was obtained from a local supplier (Sigma-Aldrich) and recrystallised from acetonitrile as colourless plates. An entire molecule of phthalazine constitutes the ASU (Figure 4.1) in the orthorhombic space group *Pbca*.

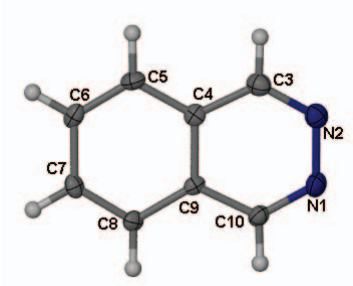

Figure 4.1 Thermal ellipsoid plot of phthalazine

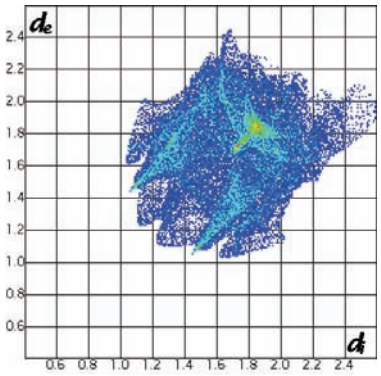

Figure 4.2 Fingerprint plot of phthalazine

The yellow-green area on the diagonal of the fingerprint plot (Figure 4.2) indicates a strong π⋯π interaction in the structure; wings, characteristic of C–H⋯π interactions, are also present, but distorted. The C–H⋯π interaction usually manifests as wings in the fingerprint plots and is often involved in the creation of herringbone motifs. However, in this instance the wings are distorted owing to the atypical sandwich herringbone motif (Figure 4.3) adopted by the phthalazine molecules. Strong intermolecular interactions are absent in the benzodiazine structure owing to a lack of strong hydrogen bond donors. The offset π⋯π interactions in the sandwich herringbone motif are supplemented by C–H⋯π and C–H⋯N interactions.

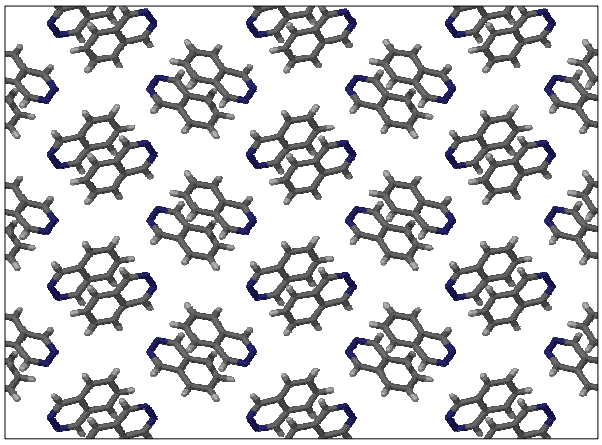

Figure 4.3 Packing diagram of phthalazine showing a single layer arranged in a sandwich herringbone motif.

4.1.2 BN3 – Quinazoline

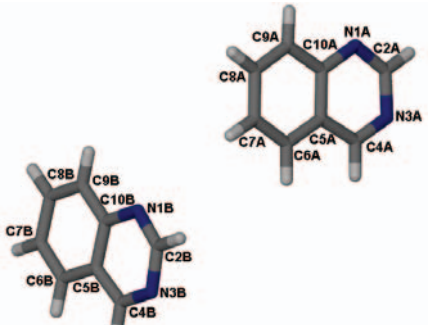

Figure 4.4 The ASU of quinazoline (QUINAZ)

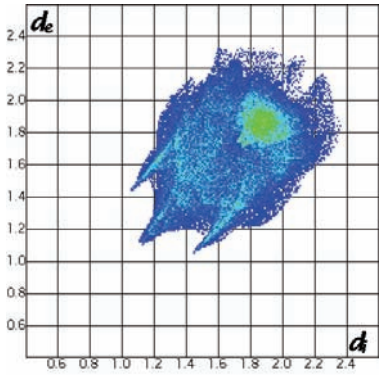

Figure 4.5 The fingerprint plot of quinazoline

The structure of quinazoline was retrieved from the CSD (Refcode QUINAZ[2]). Two symmetry-independent molecules make up the ASU (Figure 4.4) in the triclinic space group, $P\bar{1}$. The fingerprint plot (Figure 4.5) demonstrates the presence of strong C⋯C interactions that manifest as offset π⋯π stacking (green area on the diagonal at ca. 1.9 Å). Symmetry-independent molecules each pack into columns that then form layers. These symmetry-independent layers are rotated approximately 90° with respect to one another and are connected *via* weak C–H⋯N interactions.

4.1.3 BN4 – Quinoxaline

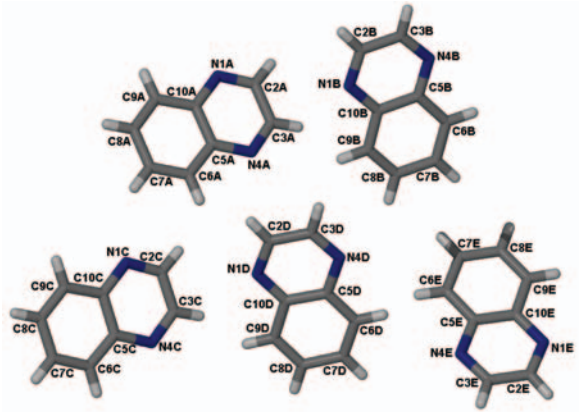

Figure 4.6 The ASU of quinoxaline (HEYJOK) contains five symmetry-independent molecules.

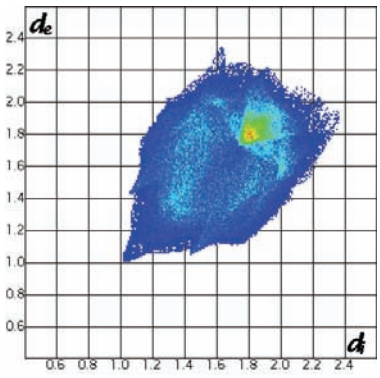

Figure 4.7 The fingerprint plot of quinoxaline

The crystal structure of quinoxaline was retrieved from the CSD (HEYJOK[3]). The compound crystallises in the orthorhombic space group, $P2_12_12_1$ with five symmetry-independent molecules present in the ASU (Figure 4.6). Each symmetry-independent molecule forms its own offset stack. The fingerprint plot verifies the presence of π⋯π

stacking with intense colouring on the diagonal at 1.8 Å (Figure 4.7). Adjacent stacks organise themselves such that molecules close-pack and the molecules of one stack are directed towards spaces in neighbouring stacks.

4.2 Co-Crystals

Eight co-crystal structures, each comprised of two complementary hydrogen bonded molecules, are presented in this chapter. Benzenediol isomers are combined with benzodiazine molecules (Table 4.1), in order to investigate the influence of an increase in molecular dimensions of one molecule, together with the possibility of increased π⋯π interactions. An second objective for the assembly of this 3×3 grid is to ascertain whether similarities present in the structures of the first grid (Chapter 3) extend into structures of the second grid.

Table 4.1 Benzenediols and benzodiazines used for co-crystallisation experiments. Blue shaded blocks indicate single-crystal structures that were elucidated, while the white shaded blocks indicate structures that have not been obtained to date.

	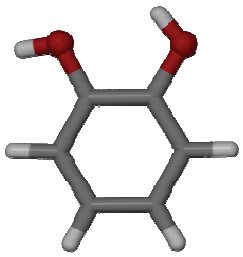	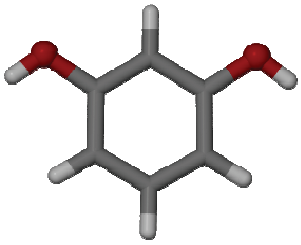	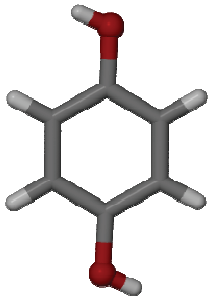
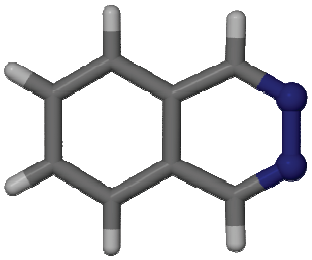	**O2BN23** 1:2	**O3BN23**	**O4BN23** 2:4
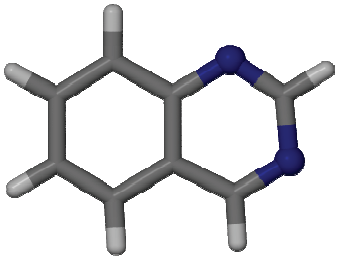	**O2BN3** 1:1	**O3BN3**	**O4BN3** ***α*** 1:2 ***β*** 2:1
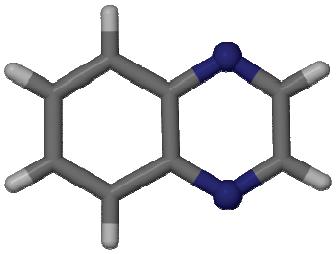	**O2BN4** 1:1	**O3BN4** 1:2	**O4BN4** in CSD: QEMKAV 1:1

4.2.1 O2BN23 – Catechol and Phthalazine 1:2

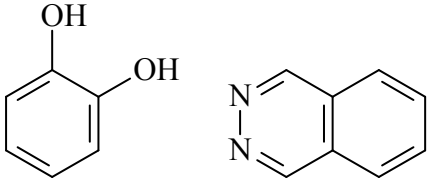

Scheme 4.2 Co-crystal formers catechol and phthalazine.

The co-crystal of catechol and phthalazine crystallises in the space group, $P2_1/c$, with two phthalazine molecules and a single catechol molecule in the asymmetric unit (Figure 4.8).

The structure was checked for missing symmetry, and none was found. Catechol adopts the *anti-anti* conformation to hydrogen bond to two phthalazine molecules on either side of the molecule *via* the O–H⋯N synthon. The resulting ternary adducts propagate perpendicular to the *ac* plane (010). Along with the strong O–H⋯N interactions, C–H⋯π and π⋯π interactions are also evident in the 3-D array and appear to contribute strongly to the organisation of the molecules, as shown by the green area along the diagonal of the fingerprint plot (Figure 4.9).

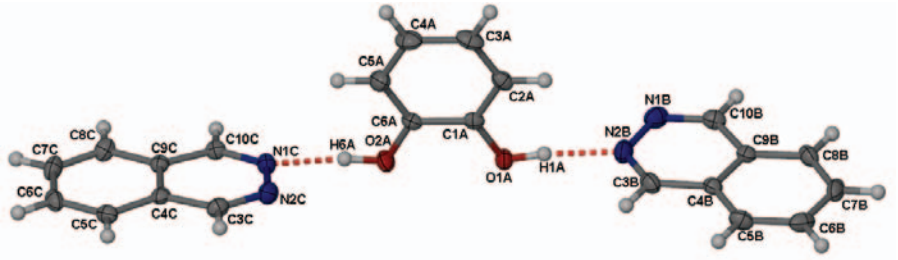

Figure 4.8 The ASU of O2BN23. Hydroxyl hydrogen atoms of catechol are in the *anti–anti* conformation. Molecules are in a similar orientation as those of *β*–O2N2 (Chapter 3).

Adducts fit together in a tongue-in-groove manner such that offset π⋯π stacking (3.667 Å) exists between phthalazine molecules oriented *anti*-parallel to one another. Molecules in each stack follow an ABAB pattern. Viewing the structure along the *a* axis (Figure 4.11) the tongue-in-groove fit of the π⋯π interactions aligns adducts into weakly connected strings.

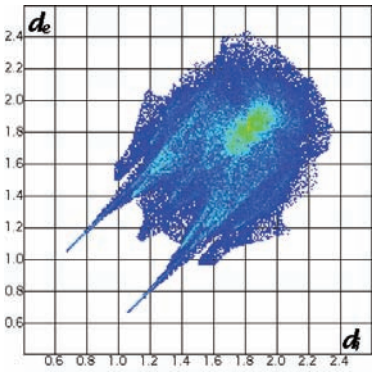

Figure 4.9 Fingerprint plot of O2BN23.

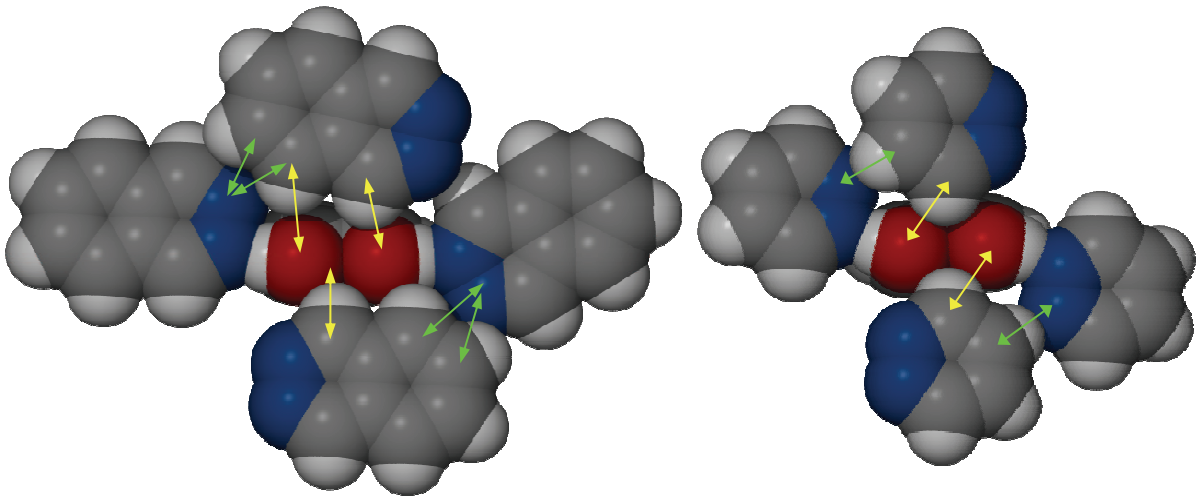

Figure 4.10 Van der Waals representation of O2BN23 (left) showing the close proximity of surrounding molecules. Yellow arrows indicate C–H⋯O interactions and green arrows indicate the C–H⋯N interactions. Further surrounding molecules have been omitted for clarity. A similar view of *β*–O2N2 is shown on the right.

Although phthalazine has two N–atoms available for hydrogen bonding, only one is used in the O2BN23 co-crystal. The unutilised N–atom takes part in C–H⋯N interactions with adjacent adducts (Figure 4.10). This situation is analogous to that in the structure of *β*–O2N2 (Chapter 3). However, the larger dimensions of the phthalazine molecule stimulate superior orbital overlap between hydroxyl oxygen atoms and C–H donors of the phthalazine ring. The larger phthalazine molecule imposes a more obtuse angle between successive adducts of O2BN23 compared to the near 90° angle of the smaller pyridazine in *β*–O2N2 (Figure 4.11). This allows increased stacking interactions between delocalised π-electrons of both rings in the fused benzodiazine rings in O2BN23.

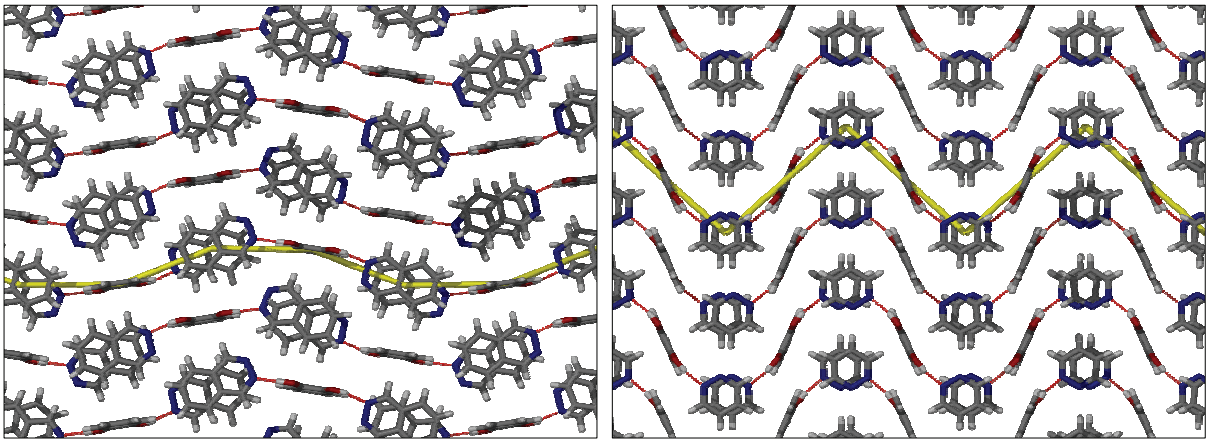

Figure 4.11 Packing diagrams of O2BN23 (left) viewed along [100] and *β*–O2N2 viewed along [001] (right) showing "chains" of hydrogen bonded adducts. The angle between adducts is noticeably different in the two structures; almost linear in O2BN23 compared to near 90° in *β*–O2N2.

The C–H⋯O interactions are thought to play a secondary role to the π⋯π interactions in steering the adducts into this arrangement. Catechol molecules in the adducts are organised

into columns stabilized by these C–H⋯O interactions. Columns are, subsequently, organised in an up-down manner along the hydrogen bonded chains (Figure 4.12).

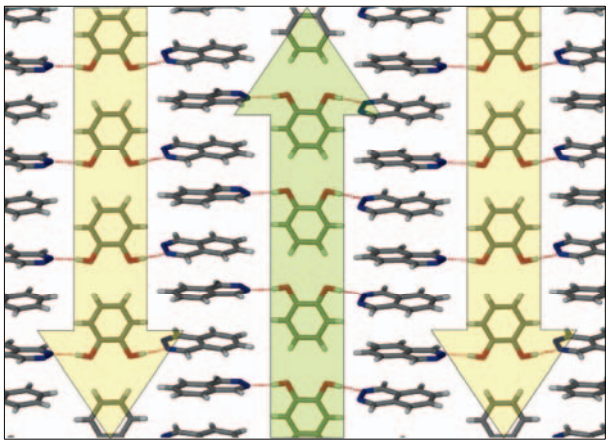

Figure 4.12 A single layer of adducts in O2BN23 is shown with catechol molecules aligned in alternating up-down pillars (indicated by shaded arrows). Phthalazine molecules stack in an offset manner, facilitating π⋯π interactions.

Since the combination O2N2 (Chapter 3) afforded two structures, one of which is similar to the structure reported here, it is arguable that the observed structure of O2BN23 is not the only possibility for co-crystallisation of catechol and phthalazine. To test this hypothesis, solvent-drop grinding experiments were carried out on three different molar ratios of catechol and phthalazine. The products of these experiments were then analysed by PXRD. Two distinct products are afforded by these preparations. A diffractogram simulated from the single-crystal data of O2BN23 (1:2 molar ratio) is comparable to that of the 1:2 molar ratio prepared by SDG (Figure 4.13) as might be expected. A single-crystal structure corresponding to the second phase (2:1) has not yet been determined. It is anticipated that this structure, if indeed it exists in a 2:1 ratio, may be similar to that of *α*–O2N2*,* forming 2:1 hydrogen bonded *hexa*-adducts. The third trace (1:1) depicted in Figure 4.13 can be ascribed to incomplete conversion of the starting material into either of the two co-crystal forms and is thus a mixture of these two co-crystals. This suggests that the initial molar ratio may be inconsequential in the preparation of either of these co-crystal forms and both may crystallise concomitantly from a 1:1 solution. Further investigation is required to determine whether this is indeed the case or whether the two forms can be inter-converted by applying specific conditions during preparation. Pure phase co-crystals can, however, be prepared by utilising the required ratio in the initial preparation. DSC analysis (Figure 4.14) of the SDG product corresponding to the single-crystal structure indicates a single event with T_{on} = 82 °C, representing the onset of single-step melting. This is only slightly lower than the melting point of the pure form components (catechol at 102 °C and phthalazine at 89 °C).

A lower melting point of the co-crystal seems counterintuitive since it implies that the co-crystal is thermally unstable in comparison to the starting materials. A more favourable heterosynthon is the basis for co-crystal formation and a lower melting point of this compound suggests otherwise.

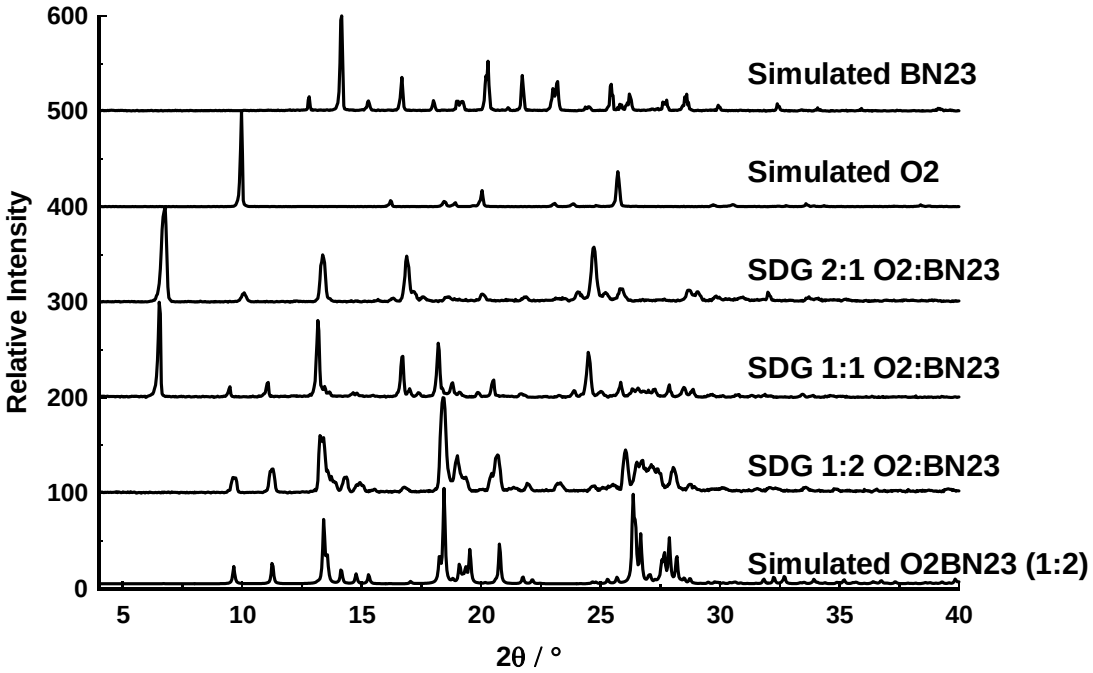

Figure 4.13 PXRD comparison of three separate SDG experiments with the simulated pattern of O2BN23 and the two starting components.

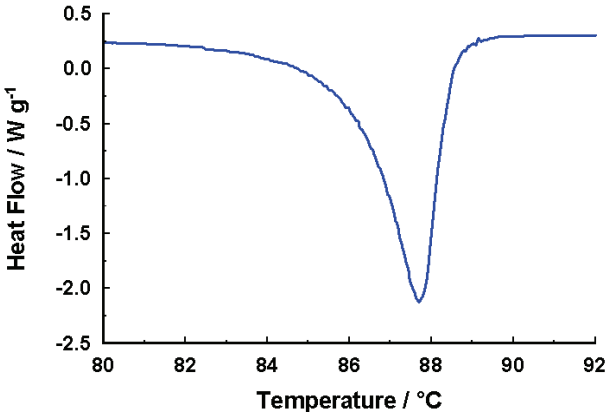

Figure 4.14 DSC trace of O2BN23**.**